The Annular Response to Tropical Pacific SST Forcing

SHUANGLIN LI, MARTIN P. HOERLING, SHILING PENG, AND KLAUS M. WEICKMANN

NOAA–CIRES Climate Diagnostics Center, University of Colorado, Boulder, Colorado

(Manuscript received 12 November 2004, in final form 20 June 2005)

ABSTRACT

The leading pattern of Northern Hemisphere winter height variability exhibits an annular structure, one related to tropical west Pacific heating. To explore whether this pattern can be excited by tropical Pacific SST variations, an atmospheric general circulation model coupled to a slab mixed layer ocean is employed. Ensemble experiments with an idealized SST anomaly centered at different longitudes on the equator are conducted. The results reveal two different response patterns—a hemispheric pattern projecting on the annular mode and a meridionally arched pattern confined to the Pacific–North American sector, induced by the SST anomaly in the west and the east Pacific, respectively. Extratropical air–sea coupling enhances the annular component of response to the tropical west Pacific SST anomalies.

A diagnosis based on linear dynamical models suggests that the two responses are primarily maintained by transient eddy forcing. In both cases, the model transient eddy forcing response has a maximum near the exit of the Pacific jet, but with a different meridional position relative to the upper-level jet. The emergence of an annular response is found to be very sensitive to whether transient eddy forcing anomalies occur within the axis of the jet core. For forcing within the jet core, energy propagates poleward and downstream, inducing an annular response. For forcing away from the jet core, energy propagates equatorward and downstream, inducing a trapped regional response. The selection of an annular versus a regionally confined tropospheric response is thus postulated to depend on how the storm tracks respond. Tropical west Pacific SST forcing is particularly effective in exciting the required storm-track response from which a hemisphere-wide teleconnection structure emerges.

1. Introduction

The leading pattern of wintertime 500-hPa height variability is hemispheric in scale and somewhat zonally symmetric in structure, having a polarity over the polar cap that is opposite in phase to that along 45°N. This annular pattern is illustrated in Fig. 1a by applying an empirical orthogonal function (EOF) analysis to January–March (JFM) monthly Northern Hemisphere 500-hPa heights. It resembles the regression of 500-hPa heights against the time coefficient of the leading EOF (EOF1) of sea level pressure (SLP), which features a more prominent zonal mean component (Thompson and Wallace 1998). In view of the coherence of the zonal mean component throughout the troposphere, Thompson and Wallace (1998; 2000) conclude that this hemispheric-wide pattern is a dynamical mode and refer to it as the Arctic Oscillation (AO), or the northern annular mode (NAM) in recognition of its distinctive zonal symmetry. The well-known North Atlantic Oscillation (NAO) is a regional manifestation of the AO.

The question has been raised whether the annular pattern is just a statistical artifact or a true dynamical mode. Deser (2000) calculated the temporal correlation between SLP anomalies at distant longitudes and found that the coherence between the midlatitude Atlantic and Pacific is weak. This lack of temporal coherence would imply that the annular pattern is a statistical artifact. A similar notion was raised by Ambaum et al. (2001) based on the comparison of the physical relevance and robustness for Northern Hemisphere variability between the AO and the NAO paradigms. As an alternate interpretation, Wallace and Thompson (2002) suggested that the lack of correlation between SLP fluctuations in the midlatitude Atlantic and Pacific stems from an interference by the second dynamical mode, the Pacific–North American pattern (PNA), and argued that the low correlation does not preclude the linkages in the annular mode. In support of this viewpoint, the

Corresponding author address: Shuanglin Li, NOAA–CIRES Climate Diagnostics Center, R/CDC1, 325 Broadway, Boulder, CO 80305-3328.
E-mail: shuanglin.li@noaa.gov

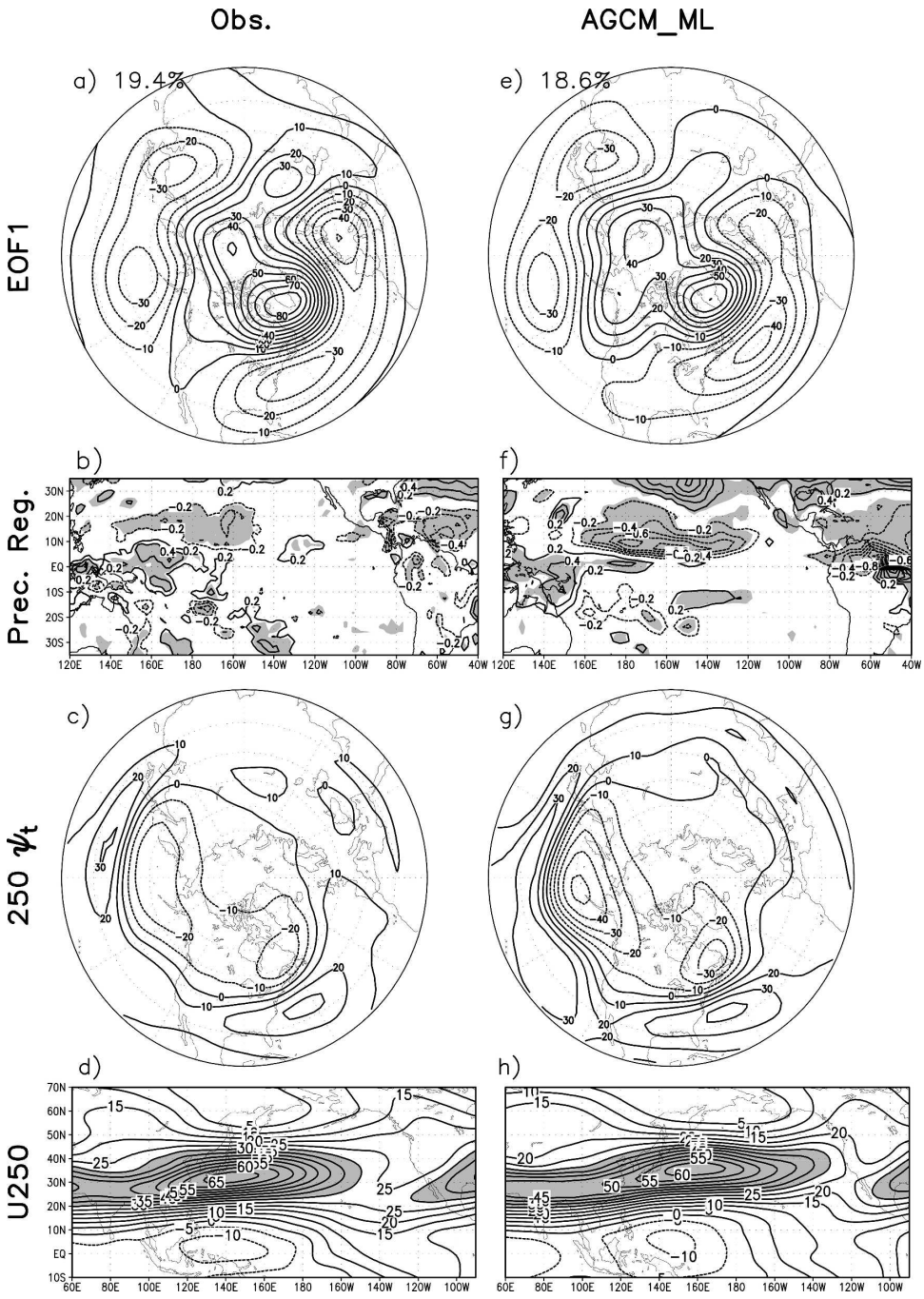

FIG. 1. Comparison of atmospheric internal variability between in the observations and in the AGCM_ML control runs. (a) The leading EOF of 500-hPa heights, (b) tropical Pacific precipitation regression on the leading EOF, (c) 250-hPa transient eddy vorticity forcing expressed by streamfunction tendency, and (d) 250-hPa nondivergent zonal wind velocity in observations. (e)–(h) Same as in (a)–(d), but in the AGCM_ML. The leading EOF explains 19.4% and 18.6% of variance, respectively. Shading represents significance at the 95% level in (b) and (f), and wind velocity greater than 30 in (d) and (h). Units: m in (a) and (e), mm day^{-1} in (b) and (f), m^2 s^{-2} in (c) and (g), and m s^{-1} in (d) and (h).

results of Branstator (2002) promote a physically based hypothesis for the existence of circumglobal patterns in which the trapping effects of the time-mean tropospheric jets act as waveguides that permit teleconnections of hemisphere-wide reach. Branstator found that these waveguide patterns possess a substantial zonal mean component, though the cause for this symmetry remains unknown.

In view of the ongoing debate over the interpretation of the annular pattern, we investigate whether the pattern can be excited physically by external forcing. If there is indeed an annular response, then one can conclude it is a dynamical structure, rather than a pure statistical artifact. Whether the annular pattern and the associated circumglobal teleconnection can be forced by tropical precipitation anomalies is also an open question raised by Branstator (2002). Therefore, the present study specifically explores whether the response to tropical heating anomalies is manifested by annular structure.

Previous observational and atmospheric general circulation model (AGCM) studies on the effect of boundary forcing on the NAO provide clues that the annular pattern may be forced by tropical Pacific sea surface temperature anomalies (SSTAs). In observational studies, east Pacific SST forcing of both the PNA (e.g., Trenberth et al. 1998) and the NAO (e.g., Pozo-Vasquez et al. 2001; 2005; Cassou and Terray 2001) has been reported. The substantial difference of observed seasonal anomalies from one ENSO event to another is consistent with this (e.g., Mathieu et al. 2004). In AGCM simulations, the NAO-like response to ENSO is also obtained (e.g., Palmer and Anderson 1994; Cassou and Terray 2001). Mathieu et al. (2004) demonstrate that the atmospheric response is sensitive to specific features of the SSTA that characterize the individual ENSO events, in agreement with Sutton and Hodson (2003). The latter show that the ENSO influence on the NAO varies during the period of 1871–1999. These diverse results may be associated with the difficulty for both the observational analyses and Atmospheric Model Intercomparison Project (AMIP) experiments to isolate the affect of the tropical east Pacific from the tropical west Pacific, since the SST in the eastern and the western basin is oppositely correlated on the interannual time scale (Rasmusson and Carpenter 1982). Our own observational analysis suggests the annular pattern to be linked to a tropical west Pacific precipitation anomaly; however, it is unclear whether this empirical association is causal. Therefore, we use model experiments to explore whether the annular pattern may indeed be forced by tropical Pacific SST forcing.

Experiments with prescribed location-varying SSTA along the equator were conducted. The primary model is a coupled GCM, an AGCM coupled to a mixed layer ocean. The results demonstrate that the 500-hPa height response to idealized SST forcing in the tropical west Pacific has a high pattern correlation with EOF1 (0.83). The response supports the argument that the annular pattern, which arises from the dynamics of purely internal atmospheric variability, may also play a role in the atmosphere's response to SST forcing. Our principal purpose is to diagnose the mechanisms for this response.

This paper is organized as follows. In section 2, the models, the experiments, and the diagnostics tools are described. Both a linear baroclinic model (LBM) and a statistical storm-track model (STM) are used to diagnose the origin of the GCM responses. In section 3, the simulated coupled responses are presented. These responses are compared with the model's internal low-frequency variability pattern. In section 4, we diagnose the mechanisms involved in the simulated response by performing LBM and STM experiments. It is discovered that the annular response cannot be explained in the framework of linear dynamics associated with the response to anomalous tropical Pacific heat sources. Instead, the dynamical feedback by transient eddies is of leading importance, and a sensitivity of the linear model response to various positions of North Pacific transient eddy forcing is found. We also examine the role of coupled air–sea feedback over the extratropical North Pacific and Atlantic Oceans for augmenting the dynamically induced annular signal. A summary and discussions are given in section 5.

2. Model experiments and diagnostics tools

a. Models and control experiments

The model used is an AGCM coupled to a slab mixed layer ocean of 50-m depth from 10°N northward to the climatological ice boundary and is referred to as AGCM_ML (Peng et al. 2005). The AGCM is an earlier version of the National Centers for Environment Prediction's (NCEP's) seasonal forecast model, with a T42 spectral truncation and 28 sigma levels. A 100-member ensemble of the AGCM_ML control runs forced with climatological seasonally evolving SST south of 10°N is adapted from Peng et al. (2005). The model was integrated for eight months (September–April) using 100 different initial conditions based on the NCEP–National Center for Atmospheric Research (NCAR) reanalysis of 0000 UTC 1–5 September 1980–99 (Kalnay et al. 1996). A similar 100-member en-

semble of uncoupled AGCM control runs is also used (Peng et al. 2002).

b. Validation of the model's intrinsic variability

Forced responses are known to be sensitive to a model's internal variability. A model with unrealistic internal variability tends to distort the atmospheric response (Peng and Robinson 2001; Hall et al. 2001). We examine if the model reproduces the observed variability. The uncoupled AGCM internal variability is similar to the AGCM_ML, so it is not discussed.

The observed leading pattern of 500-hPa height variability is extracted through an EOF analysis of January–March monthly 500-hPa heights north of 20°N. The EOFs are determined by solving a covariance matrix of height anomalies over equal-area grids. The NCEP–NCAR reanalysis from 1948 to 2000 (Kalnay et al. 1996) is used. The interannual signal associated with ENSO is removed to make the resulting EOF comparable with that derived from model control runs, which are forced with climatological seasonally evolving SSTs and thus exclude interannual variability. The process to remove the ENSO signal is performed through several steps. First, the ENSO-induced height anomaly is determined by regressing the time series of height at each grid point against an ENSO index time series. The ENSO index is defined as the area-mean SST anomaly over the domain (10°S–0°, 180°–90°W). The ENSO signal for a particular month is a product of the ENSO-associated anomaly pattern and the ENSO index for that month. The original height minus the ENSO signal yields the ENSO-removed height. The leading EOF of this residual dataset displays a zonal mean component (Fig. 1a) and resembles the 500-hPa heights regressed against the AO index (see Fig. 1 of Thompson and Wallace 1998).[1]

The link between this annular pattern and tropical heating is addressed by regressing an estimated precipitation rate against the time series of the leading EOF. We assume that the tropical heating is largely determined by precipitation and derive the latter from the reanalysis dataset. The ENSO-associated signal is also removed from the precipitation. Statistical significance is estimated from the temporal correlations of rainfall anomalies with the time coefficient of the EOF, as in Honda et al. (2001). Figure 1b shows that the observed annular pattern is associated with a tropical west Pacific rainfall anomaly. At the same time, rainfall over the tropical Indian Ocean (not shown) and west Atlantic is suppressed. The same linkage is obtained in the precipitation dataset of Xie and Arkin (1997) with a shorter data record from 1979 to 2002 (not shown).

The same EOF analysis is applied to 500-hPa heights from the 100 AGCM_ML control runs. The model's leading EOF resembles the observed one (cf. Fig. 1e with Fig. 1a) and also exhibits an annular pattern, although it accounts for slightly less variance, and its Pacific center is shifted about 10° to the south. The association of the leading model EOF with the tropical Pacific rainfall anomaly is also examined. A comparison of Fig. 1f with Fig. 1b shows that the model largely reproduces the observed association. The EOF1-associated rainfall anomaly in the model is relatively stronger, especially for the negative anomaly north of the equator around the date line.

The climatological streamfunction tendency due to synoptic-scale eddy vorticity flux convergence is also compared. It represents transient eddy forcing on the time-mean flow in steady-state mechanistic models and is referred to as transient eddy forcing or storm-track forcing (e.g., Peng et al. 2003). A "Poorman" filter is used to derive the synoptic component with time scales less than 9 days, as in previous studies (Peng et al. 2003; Li 2004). The structure of the model's storm-track forcing over the two northern oceans is largely similar to the observed (cf. Figs. 1c and 1g), although in the model it extends farther downstream over the North Pacific. This downstream extension is consistent with the downstream-extended upper-level jet, which is represented by 250-hPa nondivergent zonal wind (cf. Figs. 1d and 1h).

Since the Pacific–North American sector is sensitive to the tropical Pacific SST (e.g., Hoerling and Kumar 2002), we perform a separate EOF analysis of JFM monthly 500-hPa heights from the control runs over this regional sector (20°–87.5°N, 120°E–60°W). We then determine the hemisphere-wide height field associated with the leading regional patterns. The regression of Northern Hemispheric 500-hPa heights onto regional EOF1 (Fig. 2a) is annular and correlates with the hemispheric EOF1 regression (Fig. 1e) at 0.97. This argues a physical coherence that the hemisphere-wide structure can be treated as a dynamical mode. In comparison, the hemispheric regression on regional EOF2 is PNA-like and regionally confined. Because low-frequency patterns are primarily maintained by transient eddy forcing (Branstator 1992), intrinsic transient eddy forcings linearly linked to the two leading EOFs are also derived by regressing 250-hPa transient vorticity forcing onto the two regional EOF time series. Obviously, these two intrinsic forcings are substantially different (cf. Figs. 2b

[1] The EOF with the ENSO signal retained is very similar to Fig. 1a, except for an enhanced amplitude (~ -50 m) for the North Pacific center.

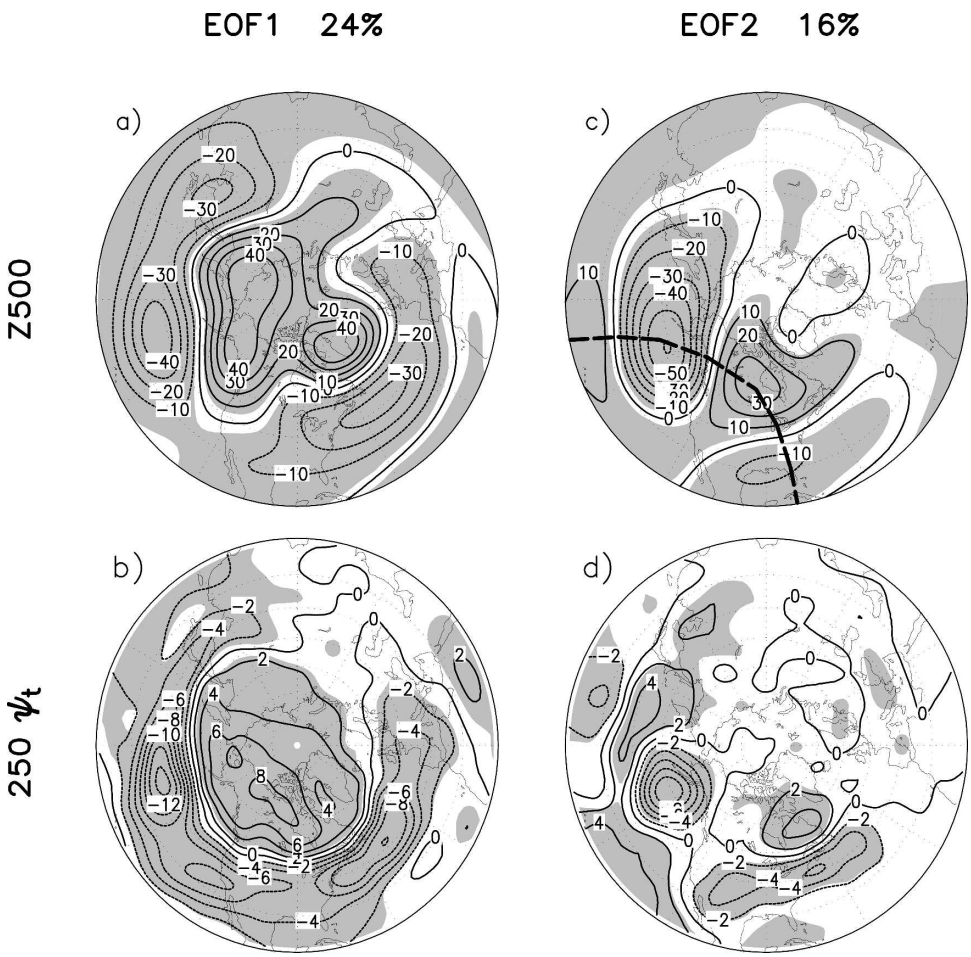

FIG. 2. Regressions of (a) 500-hPa geopotential heights and (b) 250-hPa transient streamfunction tendency onto the regional EOF1 time series of 500-hPa heights in the AGCM_ML control runs. (c), (d) Same as in (a) and (b), but for EOF2. The two EOFs account for 24% and 16% of the variance, individually. Units: m in (a) and (c), and $m^2 s^{-2}$ in (b) and (d). Shading represents significance at the 95% level.

and 2d). Similar low-frequency patterns and transient eddy forcings are obtained when we use the ENSO-removed reanalysis dataset (not shown). All these comparisons demonstrate the AGCM_ML intrinsic circulation variability is realistic and that the model can be used to investigate atmospheric sensitivity to tropical forcing.

c. Sensitivity experiments

The atmospheric sensitivity to equatorial Pacific Ocean forcing is examined by prescribing idealized SST anomalies. The idealized SSTAs used are shown in Fig. 3a. The pattern was originally motivated by the real-time development of the 2002 ENSO event. It was positioned at three different locations spanning the west to the east equatorial Pacific Ocean with centers at 155°E, 175°W, and 145°W. A comprehensive analysis of the role of equatorial SST forcing for all possible longitudes was not the purpose of our study, and previous efforts in that regard can be found in Ting and Yu (1998) and Barsugli and Sardeshmukh (2002). The main interest here is to document and understand the vastly different global response to the select forcings of Fig. 3a, despite their otherwise close proximity to each other and their identical spatial structure.

The maximum value of the idealized SSTA is 1.5°C. In the western Pacific, this value is about 2.5 times the derived monthly mean SST standard deviation in boreal winter (Fig. 3b), as estimated from the Global Ice and Sea Surface Temperature dataset (GISST; Rayner et al. 1996). Ensemble AGCM_ML runs with 60 members are conducted with these idealized SSTAs added to the seasonally evolving SST climatology. Parallel uncoupled AGCM experiments are performed to estimate

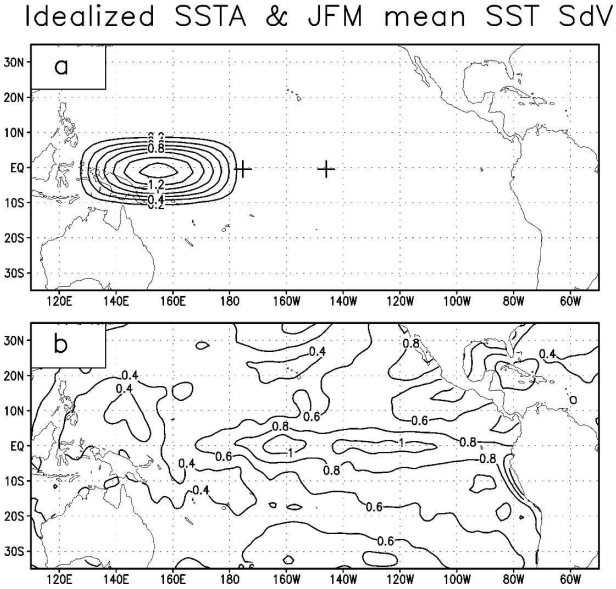

FIG. 3. (a) Idealized SSTA centered at 155°E in the equatorial Pacific. Unit: °C. The "+" represents other idealized SSTA centered at 175° and 145°W. (b) January–March mean monthly observed SST standard deviation. Unit: °C.

the influence of air–sea coupling. To further address this influence, an ensemble of 20-member AGCM runs forced with the coupled SSTA response to the idealized SSTA is also performed. For both the AGCM_ML and AGCM experiments, the model response is determined as the January–March ensemble mean difference between the forced and the control runs. A Student's *t* test is used to determine the statistical significance of the response.

d. Diagnostics tools

1) LINEAR BAROCLINIC MODEL

An LBM is used to address the maintenance and formation of the modeled response. The LBM is time dependent and based on the primitive equations. It is a global spectral model with horizontal resolution of T42 truncation and 10 equally spaced pressure levels. No topography is prescribed. One version with a lower resolution, T21, is used in Peng and Whitaker (1999). The basic state is calculated as the January–March mean of 100 AGCM_ML control runs. Rayleigh friction and Newtonian damping are given the rate of $(1\ \text{day})^{-1}$ at the lowest level and $(7\ \text{days})^{-1}$ at other levels. In addition, a biharmonic diffusion with a coefficient of $2 \times 10^{16}\ \text{m}^4\,\text{s}^{-1}$ is applied everywhere, and a thermal diffusion with a coefficient of $2 \times 10^{6}\ \text{m}^2\,\text{s}^{-1}$ is used to represent the effect of transient heat fluxes. With this dissipation and diffusion, a steady-state response is realized after about 30 days of integration. The average of the last 5 days of a 30-day integration is approximated as the linear response to a forcing.

2) STATISTICAL STORM-TRACK MODEL

The same statistical STM as Peng et al. (2003) is used. It is constructed through a multiple linear regression between the AGCM anomalous time-mean flow and anomalous transient eddy forcing in EOF space. Time-mean flow is represented by monthly geopotential heights, while eddy activity is represented by monthly streamfunction tendency due to transient vorticity fluxes with time scales less than 9 days. The linear relationship is based on the AGCM control run dataset over the northern extratropics north of 20°N. To reduce the noise, both variables are truncated to retain 40 EOFs.

3. Simulated coupled responses

Figure 4 displays the AGCM_ML simulated responses of 500-hPa heights, 250-hPa transient eddy vorticity forcing, and tropical Pacific rainfall to the idealized SSTA centered at 155°E and 145°W along the equator. The response to the 175°W SSTA appears to be a mixture of the two responses and is not displayed.

The 500-hPa height response to the west Pacific SSTA (Fig. 4a) is hemispheric with a distinct zonal mean component and projects on the model's leading EOF (Fig. 1e), although the Pacific center of the response is stronger and more localized and the northern lobe of the NAO is weaker. It also bears a projection on the northern annular mode of Thompson and Wallace (1998, see their Fig. 1). In comparison, the response to the east Pacific SSTA (Fig. 4d) is regionally confined and weaker, with almost half the amplitude. The component over the Pacific–North American sector resembles the tropical North Hemisphere (TNH) pattern of Mo and Livezey (1986). The difference between these solutions will be further quantified later when they are compared with the model's internal variability pattern.

The extratropical transient vorticity forcing (Figs. 4b and 4e) and tropical precipitation responses (Figs. 4c and 4f) are also different for the two SST forcings. The transient eddy vorticity forcing anomaly is strong and zonally extended for the west Pacific SSTA, but more localized for the east Pacific SSTA. Although the strongest transient forcing anomalies reside near the Pacific storm track in both cases, their location is somewhat shifted. The maximum transient forcing anomaly is situated around 38°N, 165°W in the west Pacific ex-

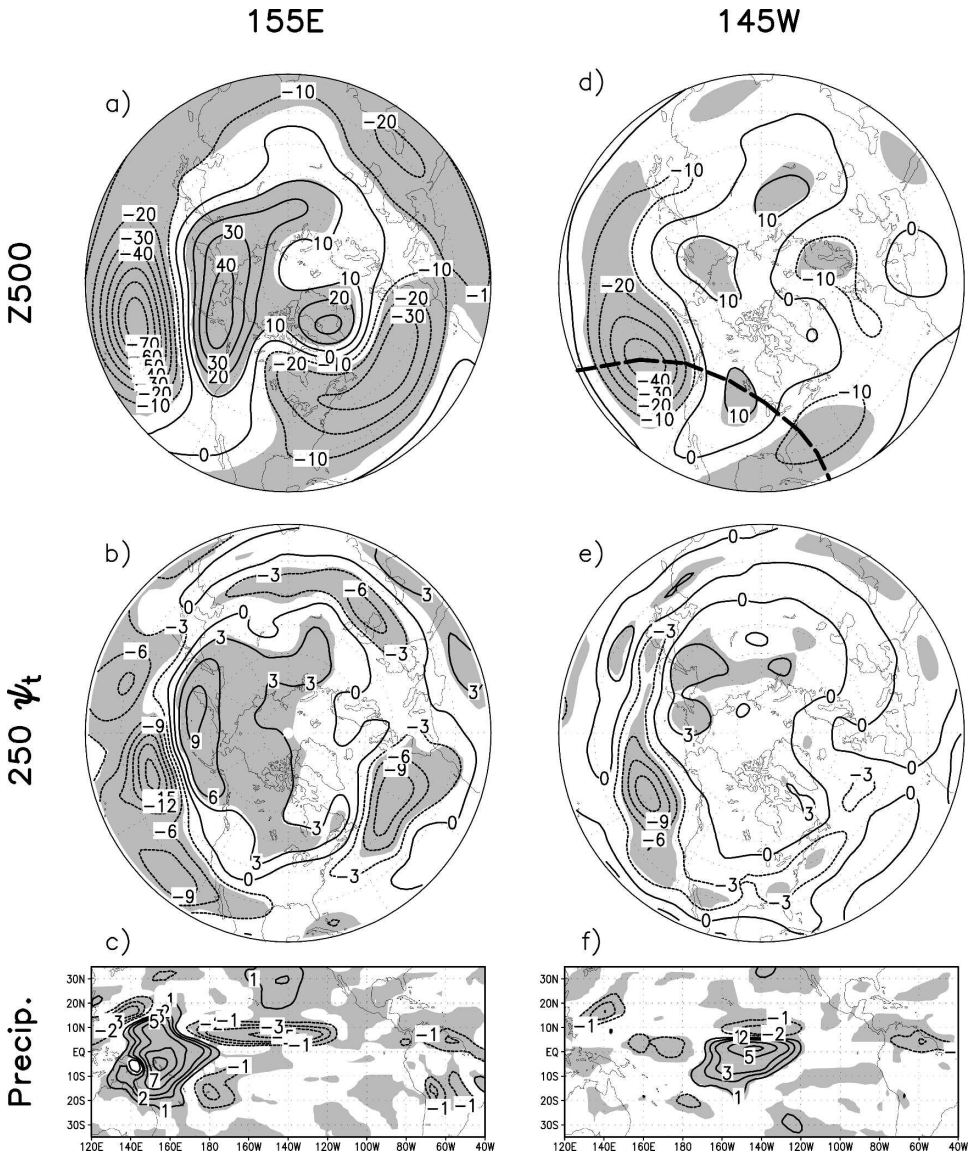

FIG. 4. AGCM_ML responses of (a) 500-hPa geopotential height, (b) 250-hPa streamfunction tendency due to transient eddy vorticity flux convergence, and (c) tropical Pacific precipitation to the 155°E SSTA. (d)–(f) Same as in (a)–(c), but to the 145°W SSTA. Units: m in (a) and (d), $m^2 s^{-2}$ in (b) and (e), and mm day^{-1} in (c) and (f). Shaded areas are significant at the 95% level.

periments, while compared to around 43°N, 155°W for the east Pacific experiments. This shift in the position of transient forcing anomalies, albeit small, is critical in understanding the origin for the two different seasonal height responses, as will be demonstrated later.

The rainfall anomaly induced by the west Pacific SSTA is an east–west dipole with the maximum over the SSTA, while the rainfall anomaly induced by the east Pacific SSTA is a north–south dipole straddling the northern margin of the SSTA. The former somewhat resembles the EOF1-associated rainfall anomaly seen both in the observations and in the model's control runs over the tropical Pacific (cf. Fig. 4 with Fig. 1), although there are significant differences away from the Tropics and over the tropical Atlantic. The tropical heating away from the Pacific may contribute to the formation of the annular pattern, as demonstrated in previous studies (e.g., Hoerling et al. 2004; Peng et al. 2005).

Previous model studies have shown that simulated responses to SSTA project on a model's internal low-frequency pattern (e.g., Peng and Robinson 2001; Hall et al. 2001; Peng et al. 2002), and we next address whether our forced solutions also project on the model's extratropical internal variability. A common fea-

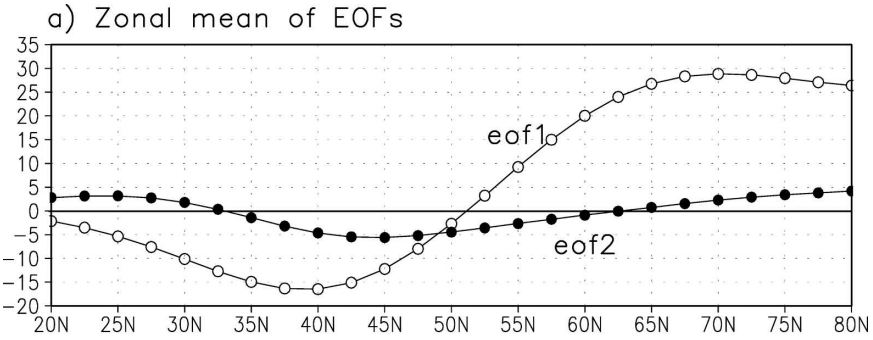

Wave	0	1	2	3	4	5	sum
EOF1 (%)	77.9	3.8	8.6	3.9	3.4	1.5	99.1
EOF2 (%)	38.8	39.4	9.4	4.7	4.6	1.7	98.6

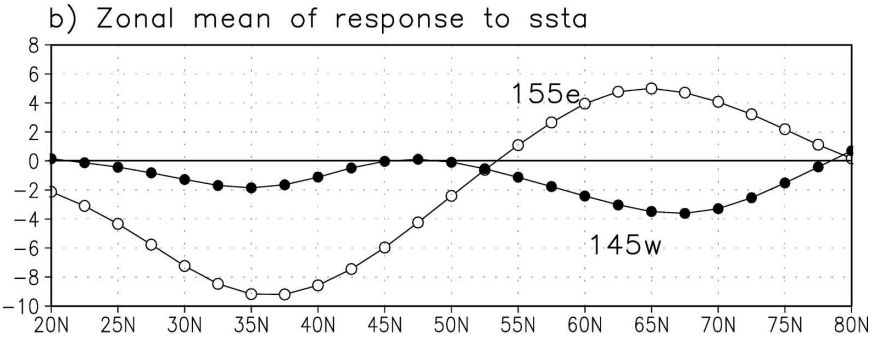

Wave	0	1	2	3	4	5	sum
155e (%)	76.1	7.1	8.7	3.6	2.0	1.7	99.2
145w (%)	50.7	22.7	4.5	5.5	10.7	4.4	98.5

FIG. 5. (a) Zonal mean of the two leading regional EOF regressions shown in Figs. 2a,c (unit: m), along with variance rate of zonal wavenumbers 0–5. The variance rate is the mean through 20°–80°N. (b) Same as in (a), but for the AGCM_ML responses shown in Figs. 4a,d.

ture of our model response to these SSTAs is a regional Pacific–North American response, which provides us a base to compare these responses with the regional EOFs of the model's intrinsic variability. The 500-hPa height responses to the west and east Pacific forcings tend to resemble the hemispheric regressions of the first and second regional EOF in the model's internal variability, respectively (cf. Fig. 4a with Fig. 2a, and Fig. 4d with Fig. 2c). The spatial correlation of the two responses with the EOF1 structure is 0.84 and 0.36, whereas with EOF2, it is 0.16 and 0.61.

To further quantify this comparison, a harmonic analysis is performed at each latitude, and the variance of individual zonal wavenumbers is computed for the two regional EOF regressions (Figs. 2a,c) and the two responses (Figs. 4a,d). Figure 5a displays the zonal mean component and the percent variance of zonal wavenumbers 0–5 for the two EOF regressions. The EOF1 has a strong zonal mean component, which accounts for 77.9% of the total variance. In contrast, the zonal mean in the EOF2 is much weaker and accounts for only 38.8% of the variance. The EOF2 regression is largest for wavenumber 1. For the response (Fig. 5b), the zonal mean component dominates the response to the west Pacific forcing and accounts for 76% of total variance. In contrast, wavenumber 1 is a statistical feature of the response to the east Pacific forcing. Tropical west Pacific SST anomalies thus excite a markedly different atmospheric sensitivity, one that tends to select the leading annular EOF of internal variability. When the model transient eddy responses are compared with the model's internal transient eddy forcing associated with the two EOFs (cf. Fig. 4 with Fig. 2), they exhibit a similar correspondence. These results indicate that the annular pattern, which arises from the dynamics of purely internal atmospheric variability, may play a role

in the atmospheric response to tropical west Pacific SST forcing.

4. Mechanism diagnostics

a. Atmospheric sensitivity to Pacific transient eddy forcing

The convergence of transient eddy vorticity fluxes and diabatic heating are known to be the primary processes maintaining low-frequency circulation patterns (e.g., Branstator 1992). Transient eddy vorticity forcing is computed from daily u- and v-wind output at vertical pressure levels of model output. Diabatic heating was derived from daily outputs of the model's sensible and latent heating and radiation flux. The difference of these forcings in the SSTA experiments and the control experiments represents the anomalous forcing induced by the SSTA. The relative importance of the two forcings in maintaining the model response can be determined with the LBM experiments with these individual anomalous forcings. A steady LBM solution represents the atmospheric response to the steady anomalous forcing. Our results (not shown) demonstrate that, for these two SSTA cases, the transient eddy forcing is dominant in maintaining the AGCM_ML response, in agreement with previous studies (e.g., Peng et al. 2003; Lau and Nath 1991). The spatial correlation of the LBM response to transient eddy forcing (heating) with the AGCM_ML response is 0.79 and 0.75 (0.04 and 0.13) for the two SSTA cases.

As noted previously, the transient eddy forcing that maintains the two different response patterns in the AGCM_ML exhibits maxima over the North Pacific, but in slightly different locations (see Figs. 4b and 4e). The forcing induced by the west Pacific SSTA is situated in the core of the jet exit, while the forcing induced by the east Pacific SSTA is shifted 5° northward and 10° downstream. Branstator (2002) demonstrated that vorticity sources at different locations relative to the jet core may induce different responses. Because of the waveguide effects of the Pacific jet (Hoskins and Ambrizzi 1993), disturbances near the jet core tend to be meridionally confined to the vicinity of the jet and propagate farther in the zonal direction, resulting in zonally oriented chains of anomalies. Branstator further suggested that disturbances confined to the vicinity of the jet contribute to the formation of the annular mode. In contrast, disturbances away from the jet core, where there are weak meridional gradients of background vorticity, tend to propagate meridionally, resulting in a prominent meridionally arched structure with less zonal extent. This waveguide mechanism may be instrumental in understanding our two different responses to tropical Pacific SSTAs. We address this question by examining the LBM response to an idealized transient eddy vorticity forcing and the sensitivity to its location relative to the Pacific jet.

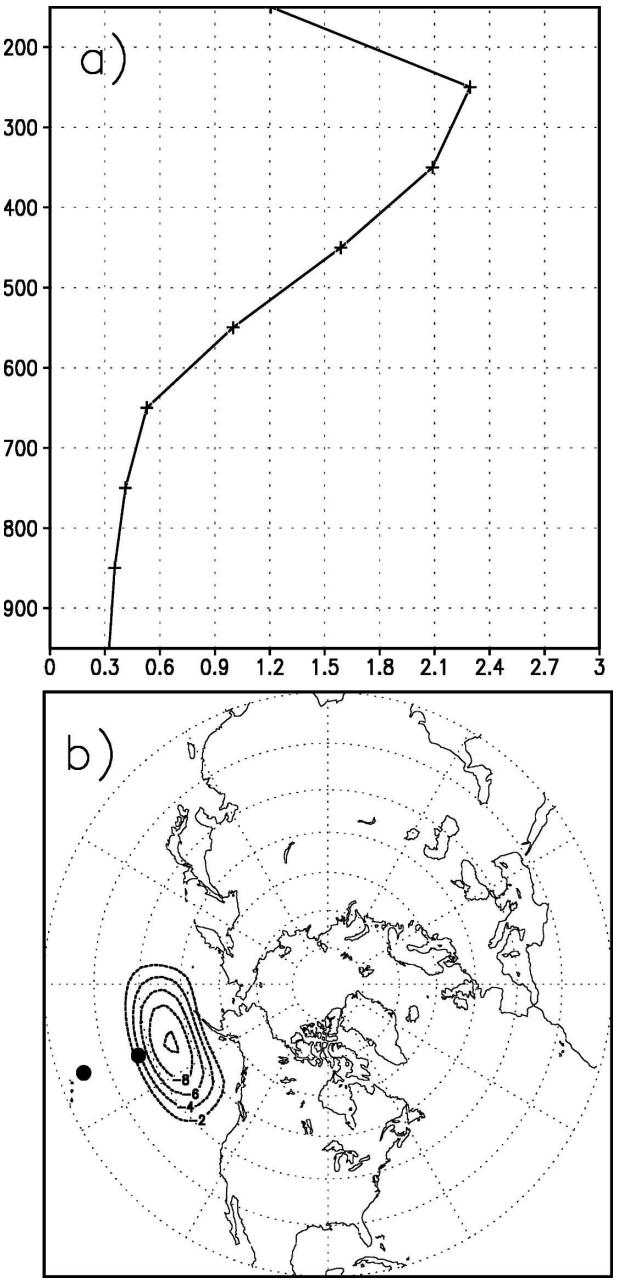

FIG. 6. (a) Vertical profile and (b) in-depth mean of an idealized Pacific transient eddy vorticity forcing centered at 45°N, 160°W. The transient forcing is expressed as streamfunction tendency. Unit: $m^2 s^{-2}$. The mark "●" in (b) stands for the location of forcing centered at 38°N, 160°W and 25°N, 160°W.

An idealized transient eddy vorticity forcing is defined as shown in Fig. 6 and is roughly based on the maximum North Pacific transient forcing responses in

TABLE 1. Spatial correlations of LBM 500-hPa height responses to an idealized forcing centered at different positions with the two leading EOF regressions displayed in Figs. 2a,c (noted as ^EOF1 ^EOF2, respectively). The coefficients greater than 0.6 are in bold type. The spatial domain to calculate the correlation with the EOF1 is over the Northern Hemisphere north of 20°N, and over the PNA sector (20°–90°N, 150°E–30°W) for the correlations with the EOF2. The numbers in italics indicate that the correspondent responses have been displayed in Fig. 7.

		180°	175°W	170°W	165°W	160°W	155°W	150°W	145°W
45°N	^EOF1	0.14	0.18	−0.19	−0.16	*−0.10*	0.04	0.13	0.25
	^EOF2	**0.77**	**0.75**	**0.74**	**0.73**	***0.71***	**0.68**	**0.62**	0.55
38°N	^EOF1	**0.76**	**0.75**	**0.73**	**0.72**	***0.71***	**0.71**	**0.70**	**0.69**
	^EOF2	0.17	0.22	0.27	0.29	*0.29*	0.27	0.24	0.21
25°N	^EOF1	−0.48	−0.44	−0.39	−0.33	−0.27	−0.21	−0.16	−0.11
	^EOF2	−0.50	−0.56	**−0.61**	**−0.64**	**−0.64**	**−0.63**	**−0.60**	−0.57

the AGCM experiments. Modest modifications to the shape of the idealized transient forcing do not result in a qualitative difference in the LBM response. We perform suites of experiments in which the center of the idealized transient forcing is shifted zonally from the date line to 145°W and shifted meridionally between 38° and 45°N to sample the range of locations of the two transient forcing maximum induced by the tropical Pacific heating. The transient forcings positioned along 38°N reside closer to the Pacific jet core, whereas those along 45°N are relatively poleward of the jet core (cf. Fig. 6b with Fig. 1h). To verify the jet waveguidance mechanism, additional LBM experiments with the idealized transient forcing positioned south of the jet along 25°N are conducted.

Overall, the LBM response to the idealized transient forcing tends to project on an annular pattern when the forcing resides closer to the jet core, and on a more regional response when the forcing is positioned away from the jet core. This is summarized in Table 1 using the spatial correlations between the LBM 500-hPa height responses and the model's two leading regional EOF regressions (Figs. 2a,c). In general, the correlations of the LBM responses with the EOF1 (EOF2) regression are greater (less) than 0.6 when the forcings are positioned along 38°N, and less (greater) than 0.6 when the forcings are positioned along 45°N. The response to the forcing along 25°N is similar to that along 45°N but has an opposite sign.

To illustrate the spatial structure, Fig. 7 displays the LBM 500-hPa height response to the idealized transient forcing centered at 38°N and at 45°N along 160°W. The response to the 38°N forcing is hemispheric and possesses an apparent zonal mean component having out-of-phase anomalies between 40°N and the polar cap. By contrast the response to the 45°N forcing is confined to the Pacific–North American sector, with negligible zonal symmetry. When compared with the AGCM_ML forced responses (see Figs. 4a,d) and the model's two leading internal EOFs (Figs. 2a,c), the LBM response to the 38°N forcing resembles the AGCM_ML response to the west Pacific SSTA (Fig. 4a) by a pattern correlation coefficient of 0.6, and the EOF1 pattern (Fig. 2a) by 0.7 (see Table 1). Moreover, the LBM response to the 45°N forcing resembles the AGCM_ML response to the east Pacific SSTA (Fig. 4d) by 0.5, and the EOF2 pattern (Fig. 2c) by 0.7 (see Table 1). The resemblance includes agreement in the spatial structure, and in the relative contributions from their zonal wavenumber components (cf. Fig. 7 and Fig. 5). Therefore, for our cases, the latitudinal difference in the transient eddy forcing appears to be most instrumental in shaping the two different responses to tropical Pacific forcing.

To better understand the difference in the LBM responses, we examine the time-dependent atmospheric adjustment to the two idealized transient forcings. The upper and middle panels in Fig. 8 suggest that the height response to the two forcings begins to bifurcate around day 3. The 38°N forcing induces strong height anomalies propagating into and across the polar cap. It yields a south–north dipole over the North Pacific within 3 days and then propagates downstream farther and develops into a hemispheric signal with an annular component within 10 days. The downstream propagation is seen more obviously in the 200-hPa meridional wind velocity plots (lower panels of Fig. 8). In contrast, the 45°N forcing induces height anomalies propagating to the south, and then becomes trapped in the midlatitude of the PNA sector. This suggests that the poleward and downstream propagation of the response may be key in inducing the annular pattern, although the underlying mechanism needs to be understood further.

The robustness of the LBM sensitivity was tested by repeating the calculations, but linearized about the observed climatological basic state. The observed basic state is derived from the NCEP–NCAR reanalysis. Largely similar responses are obtained for the three forcings along 160°W (not shown). The consistency of the results under the two basic states suggests that the

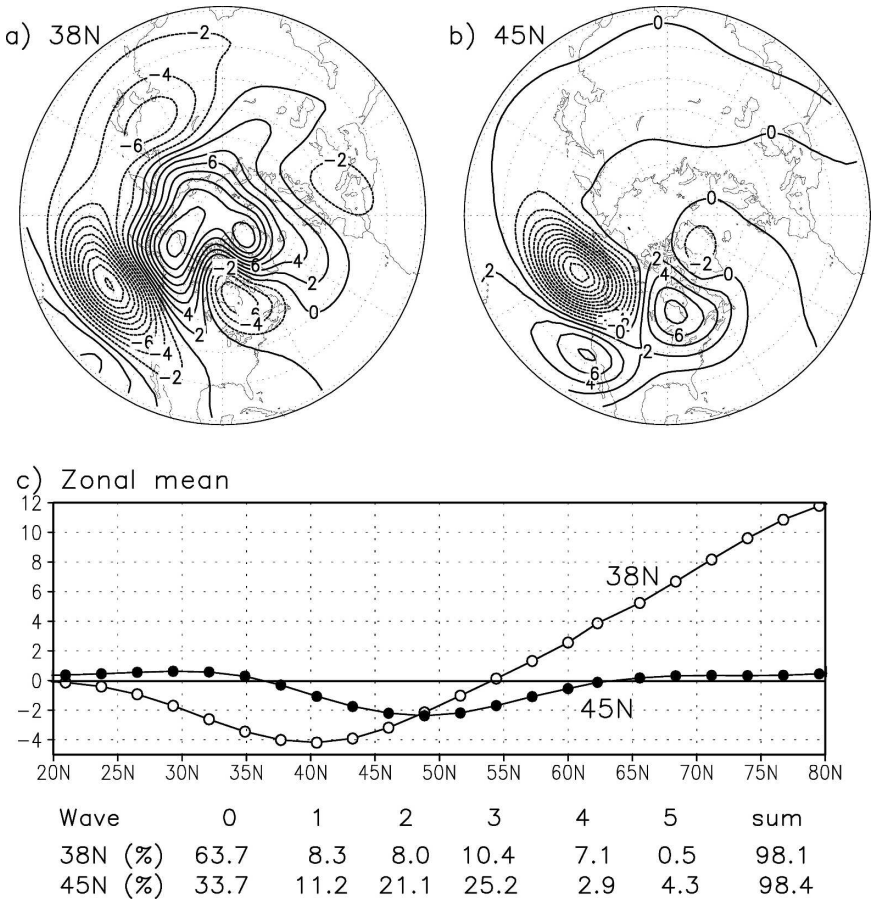

Wave	0	1	2	3	4	5	sum
38N (%)	63.7	8.3	8.0	10.4	7.1	0.5	98.1
45N (%)	33.7	11.2	21.1	25.2	2.9	4.3	98.4

FIG. 7. LBM 500-hPa height response to the idealized Pacific transient eddy forcing shown in Fig. 6: (a), (b) for the forcing with the maximum at 38° and 45°N along 160°W, individually. (c) The zonal mean of the responses displayed in (a) and (b), along with the variance rate of wavenumbers 0–5. Unit: m.

sensitivity of the response pattern to the position of transient forcing relative to the Pacific jet is robust.

b. Role of dynamical interaction between time-mean flow and transients over the Atlantic

One may note that, although the LBM response to the transient forcing at 38°N is well correlated with the annular pattern, the response component over the North Atlantic is neither a typical NAO, nor does it resemble the AGCM_ML response to the 155°E SSTA. In particular, there is not a well-defined southern lobe in Fig. 7a. One needs to keep in mind that this LBM response is induced only by the North Pacific transient forcing, without including the effect of feedback between time-mean flow anomaly and transient eddy activity over the North Atlantic. In the AGCM_ML, as well as in nature, the North Atlantic anomalous time-mean flow induced by the Pacific transient forcing will interact with the storm track locally. This transient response to the time-mean flow anomaly can be estimated by using an STM (e.g., Peng and Whitaker 1999; Peng et al. 2003; Li 2004).

Using the North Atlantic height anomaly forced by the idealized Pacific transient forcing at (38°N, 160°W), Fig. 9a displays the corresponding STM-predicted transient eddy forcing. There is a dipolelike transient eddy forcing anomaly over the North Atlantic, one that is qualitatively similar to the equilibrated transient forcing anomaly of the west Pacific SSTA runs (see Fig. 4b). The feedback of this Atlantic transient forcing on the time-mean flow is in turn estimated by the LBM. Figure 9b shows that the LBM response to the anomalous North Atlantic transient forcing features a phase-reversed NAO-like dipole. In comparison with the response induced remotely by the idealized Pacific transient forcing (Fig. 7a), the local eddy feedback over the Atlantic resembles the NAO with a clear southern lobe. Since the present LBM response tends to underesti-

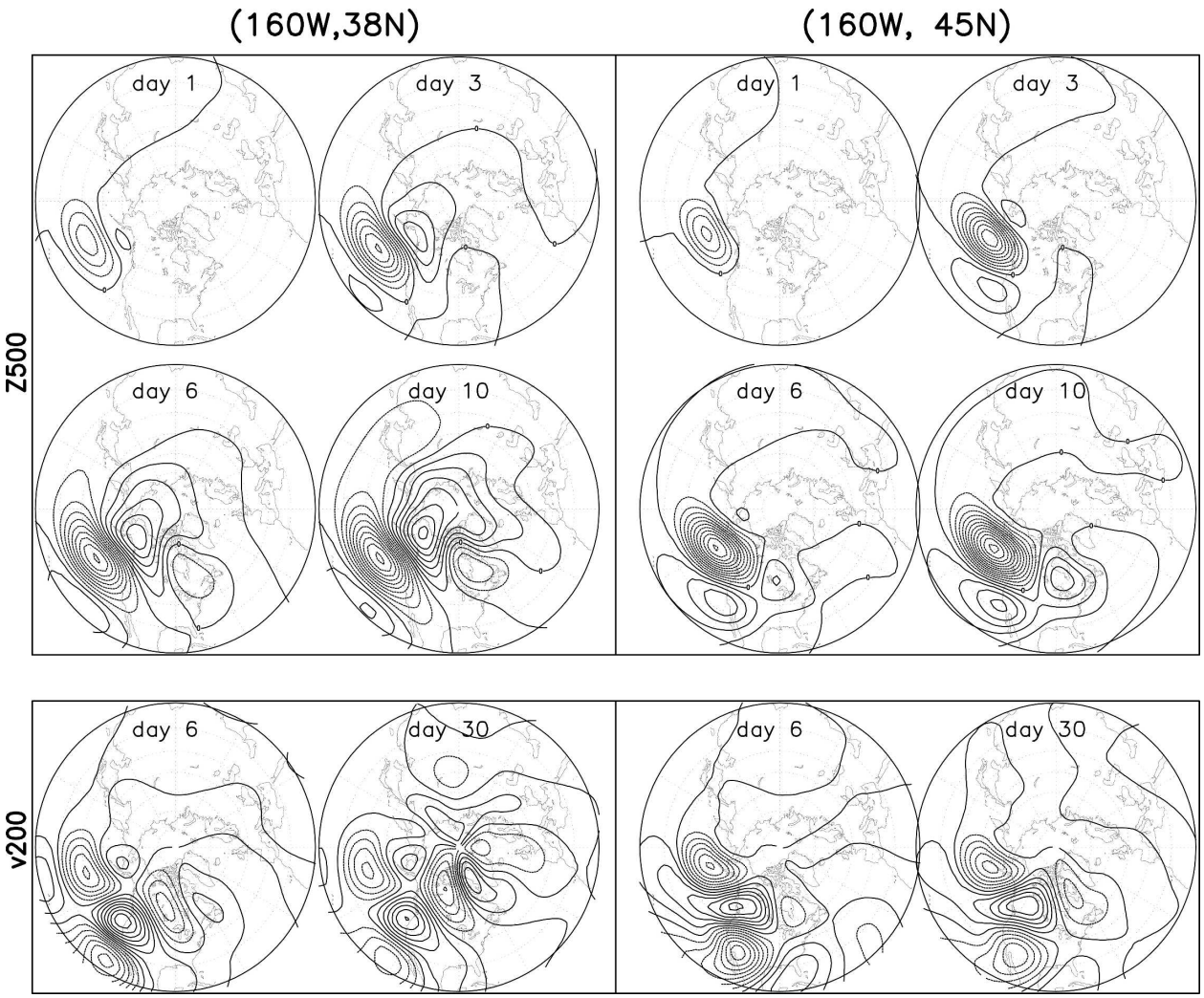

FIG. 8. (top) Same as in Figs. 7a,b, but time-dependent response on days 1, 3, 6, and 10, respectively. Interval of contour: 2 m. (bottom) The 200-hPa meridional wind velocity on days 6 and 30. Interval of contour: 0.2 m s^{-1}.

mate the response to a forcing and shift the response somewhat northward (Peng et al. 2003), we surmise that the local eddy feedback is probably stronger than can be diagnosed with our interactive approach of sequentially applied damped linear models. Nonetheless, our analysis demonstrates that the local interaction between time-mean flow anomaly and eddy transience over the North Atlantic acts to enhance an NAO-like response. With further interaction of the time-mean flow and eddies, an anomalous equilibrium state may project more on the annular pattern.

c. *Impact of extratropical air–sea interaction*

Another factor that influences the extratropical atmospheric response to tropical Pacific forcing is the extratropical air–sea interaction. We estimate this influence by comparing the uncoupled with the coupled response. The uncoupled 500-hPa height response bears a resemblance to that in the coupled runs (cf. Fig. 10 and Fig. 4). The spatial correlations between the uncoupled and coupled responses are 0.94 and 0.87 for these two SST forcings, respectively. However, the uncoupled responses are considerably weaker. There is a significant coupling-induced increase for the 155°E SSTA. But, generally the effect of coupling does not substantially alter response patterns. The coupled–uncoupled difference is well correlated with the coupled responses at 0.79/0.64 for the 155°E/145°W SSTA. Correspondingly, the mixed layer's extratropical SST response to the west Pacific SSTA is stronger than for the east Pacific SSTA. Note that, in the North Atlantic, there is a tripole SST response to the west Pacific

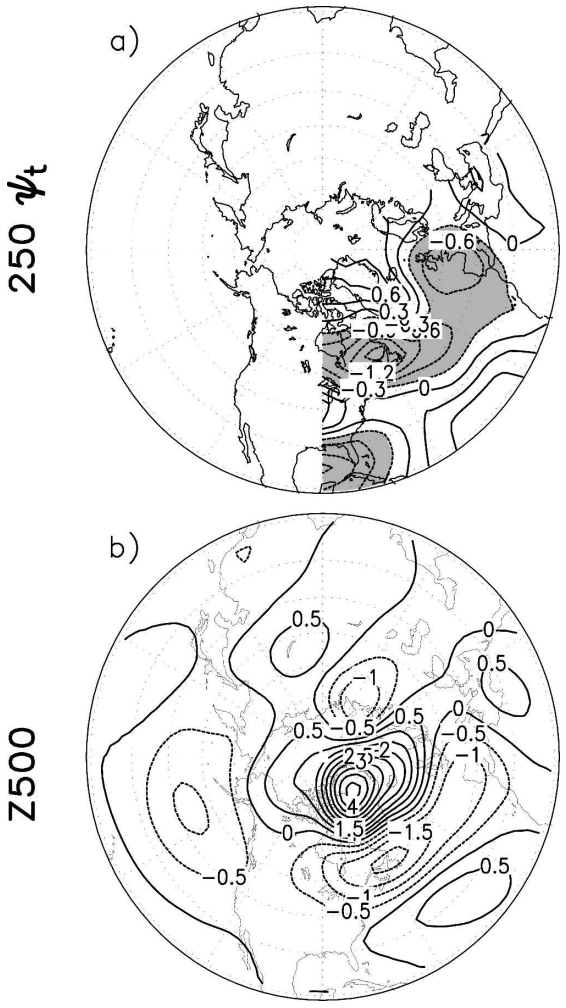

FIG. 9. (a) STM-predicted transient eddy forcing response to the North Atlantic anomalous flow in Fig. 7a. Shading indicates values less than –0.3. (b) LBM response to the anomalous transient forcing in (a). Unit: $m^2 s^{-2}$ in (a), and m in (b).

SSTA (Fig. 10b) but virtually no significant SST response to the east Pacific SSTA (Fig. 10e). Since an SST tripole can both be forced by the NAO and also force an NAO-like anomaly (Rogers 1997; Rodwell et al. 1999; Sutton et al. 2000; Peng et al. 2002), air–sea interactions apparently enhance the annular response to the 155°E SSTA in the AGCM_ML. To verify this point, the coupled SST response (Fig. 10b) to the 155°E SSTA is added to the climatological seasonally evolving SST to perform additional AGCM experiments. Figure 10f shows that this forced SST response induces a 500-hPa height response with the strength close to the difference between the coupled and the uncoupled difference (Fig. 10c), and it also exhibits a zonal mean component. Thus, the extratropical air–sea interaction has substantially amplified the response projection on the annular mode. The deficient amplitude of the North Atlantic response induced by Pacific transients is substantially enhanced through the local extratropical air–sea feedback.

5. Summary and discussions

Observations indicate the leading EOF of 500-hPa heights, an annular pattern, is associated with the tropical western Pacific heating, and we explore whether SST variations in that region may be effective in inducing an annular response. A coupled GCM is employed to investigate atmospheric responses to tropical Pacific forcings, and its sensitivity to various forcing locations. Experiments with idealized SSTAs centered at different locations on the equator were carried out. The model response to the west Pacific SSTA exhibited a hemispheric pattern projecting on the annular mode, while the response to the east Pacific SSTA exhibited a weaker, localized pattern. These two different responses project on two corresponding structures of model internal variability. Parallel experiments using an uncoupled AGCM demonstrated a similar but weaker response to those tropical Pacific SSTAs. Therefore, there is a significant contribution from the tropical west Pacific to the annular mode, and local extratropical air–sea feedback acts to enhance the annular response to the tropical western Pacific forcing.

We sought to understand the physical processes responsible for the annular response and also the reasons for a lack of such a response to east Pacific forcing. The relative roles of diabatic heating and transient eddy forcing in the maintenance of the two responses were investigated using a linear diagnostic model. Our results indicated that both extratropical responses were maintained predominantly by transient eddy vorticity forcing. The transient eddy forcing in both cases exhibited a maximum over the North Pacific, but with different meridional positions relative to the upper jet. The atmospheric sensitivity to an idealized Pacific transient forcing with various locations relative to the upper jet was explored with further LBM experiments. This latter difference was judged to be critical in differentiating annular from PNA sector–confined responses. Our results showed that transient forcing near the jet core, as induced by the tropical west Pacific SSTA, tended to induce an annular response, whereas the forcing relatively away from the jet core induced a regionally trapped response. The Pacific eddy-induced annular response was then found to be further enhanced by the North Atlantic local interaction between time-mean flow and transient eddies.

In view of the atmospheric sensitivity to the Pacific

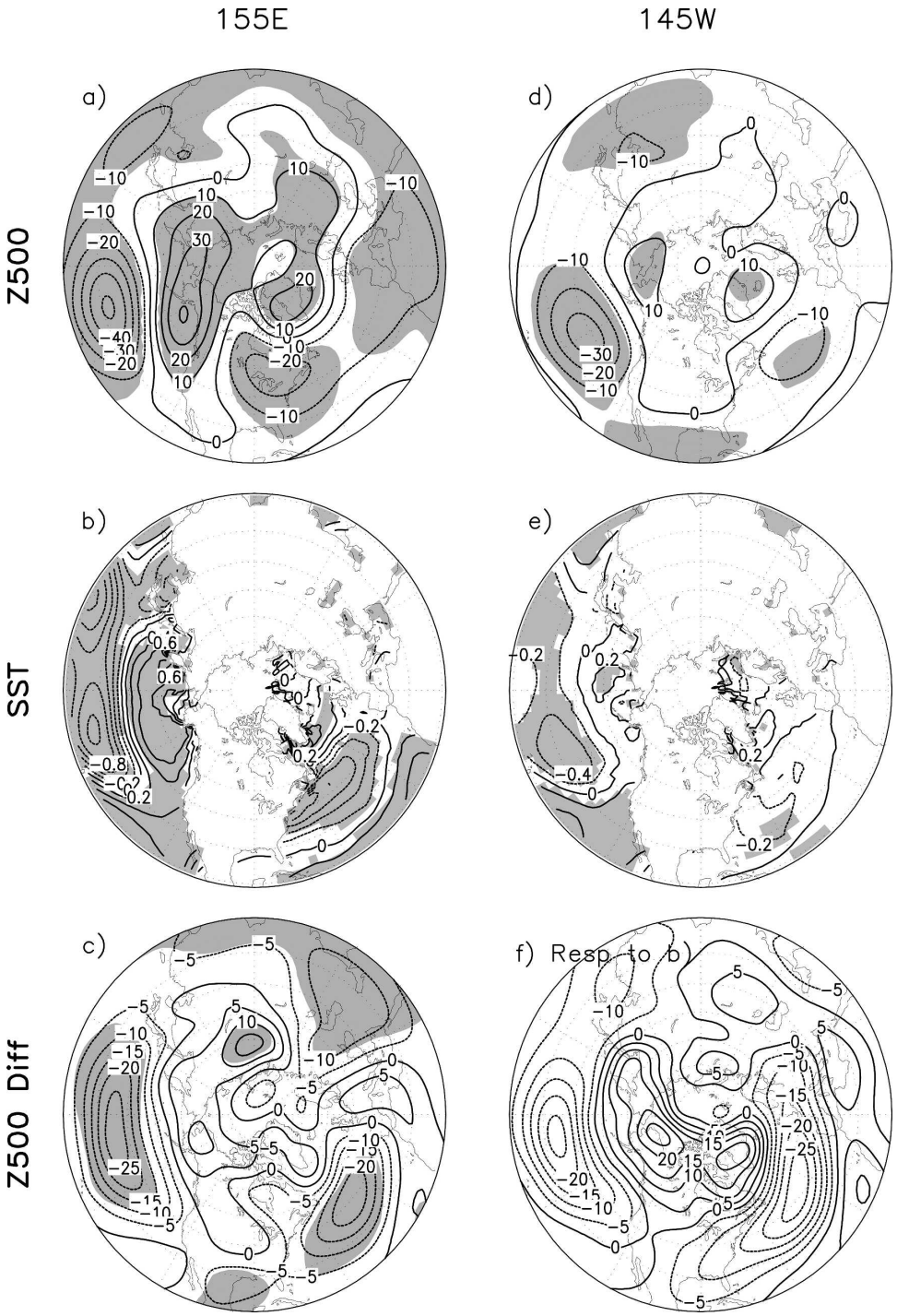

FIG. 10. (a) The AGCM 500-hPa height response, and (b) the AGCM_ML coupled extratropical SST response to the 155°E SSTA. (c) The difference of the coupled responses in Fig. 4a minus the uncoupled 500-hPa height responses in (a). (d), (e) Same as in (a) and (b), but for the 145°W SSTA. (f) the AGCM 500-hPa height response to the forced coupled SSTA in (b). Units: m in (a), (c), (d) and (f), and °C in (b) and (e). Shaded areas are significant at the 95% level.

transient eddy forcing, an important question is the origin of the difference in the latitudinal location of the transient forcing. Within the paradigm of tropical–extratropical interactions, tropical heating initially forces an extratropical anomaly through the vorticity flux convergence generated by heating-induced irrotational flow (Sardeshmukh and Hoskins 1988). This heating-induced time-mean flow anomaly subsequently acts on midlatitude storm tracks and acts to organize transient eddies. Figure 11 displays time-dependent LBM 200-hPa height responses to an idealized elliptical heating centered at 155°E in vicinity of the AGCM_ML rainfall response to our tropical west Pacific SSTA (left panels), and also to identical heating at 145°W corresponding to the east Pacific SSTA-induced rainfall (right panels). Two key differences in extratropical height responses to the two heatings are already seen by day 6. First, the response to 155°E heating is about 1.5 times as strong as that to 145°W heating. This may partially explain why the AGCM_ML response to the 155°E SSTA is stronger than that to the 145°W SSTA. Second, the location of the North Pacific negative height response to the 145°W heating is shifted downstream by ~20 longitude degrees and northward by ~5 latitude degrees. These additional calculations reveal the sensitivity of extratropical responses to tropical heating locations, consistent with previous linear model studies (e.g., Ting and Sardeshmukh 1993; Ting and Yu 1998). It is our interpretation drawn from extensive experiments that such a difference, though modest, is critical for understanding the fully equilibrated response that includes transient eddy adjustment and their nonlocal feedbacks, which can yield annular solutions. Such a difference argues for the existence of a different latitudinal location of transient forcing induced by the west and the east Pacific tropical heating. But this is not simulated well by our tentative STM experiments and needs further investigation.

Figure 12 summarizes our understanding of the processes responsible for the different responses to the two SSTAs in the AGCM_ML. First, the anomalous heatings located in the west and in the east Pacific both induce arched extratropical height anomalies across the Pacific–North American sector, with a maximum negative anomaly over the North Pacific. There is a small difference in the strength and location of the Pacific negative anomaly between the two heatings. The resulting anomalous flow modulates the transient eddy activity and induces an anomalous transient forcing, with a maximum near the exit of the Pacific upper jet. The strength and location of this maximum transient eddy forcing is slightly different. The transient forcing induced by the tropical west Pacific heating is stronger and resides in the jet core, while that induced by the east Pacific heating is weaker and removed from the jet. Perturbations induced by the transient forcing within the jet core tend to propagate poleward and also downstream, and develop into a strong and hemispheric pattern projecting on the annular mode. The Atlantic sector anomalous flow induced by the Pacific transient forcing will further interact with the storm track locally, enhancing an NAO-like response and the annular component. The extratropical air–sea interaction will further enhance this structure. Perturbations induced by the transient eddy forcing away from the jet core tend to propagate southward and eastward and induce an arched response.

Here we have provided independent evidence for the physical realism of the annular pattern, having a distinctive feature of strong zonal symmetry. Our results support the interpretation that the empirically derived EOF1 is not a statistical artifact. The model experiments further established that particular patterns of SST forcing in the Tropics may tend to select an annular response, though our analysis has not exhaustively studied all tropical sources of such variability. Tropical Indian Ocean heating can also force an annular response (Hoerling et al. 2004).

We prescribed an idealized Pacific transient eddy forcing and obtained atmospheric sensitivity to the latitudinal, but not the longitudinal, location of the forcing. This lack of sensitivity to the longitudinal location may be related to the excessive downstream extension of the model's Pacific upper jet (see Fig. 1h), since the group velocity of barotropic Rossby waves is proportional to the meridional gradient of background absolute vorticity (Hoskins and Ambrizzi 1993). A modest atmospheric sensitivity to longitudinal location of transient forcing may also exist in nature, as demonstrated in Branstator (2002). One may question the validity of prescribing an idealized localized transient eddy forcing, since the transient forcing actually induced by tropical heating is more complicated. Additional experiments suggest that, when the complete transient forcing induced by the tropical west and east Pacific heating is used, the difference of the LBM responses is still distinguishable, albeit not as distinctly as with the idealized localized forcing. Another question concerns the validity of diagnosing the global transient eddy feedback via a sequence of linear solutions. Under a linear scenario, for a constant basic flow, the LBM mean response to all combined eddy forcings should be equal to the sum of the individual forcings. This indicates that, when transient-induced response is small relative to the basic flow, this process is valid. In the present study all transient-induced vorticity responses

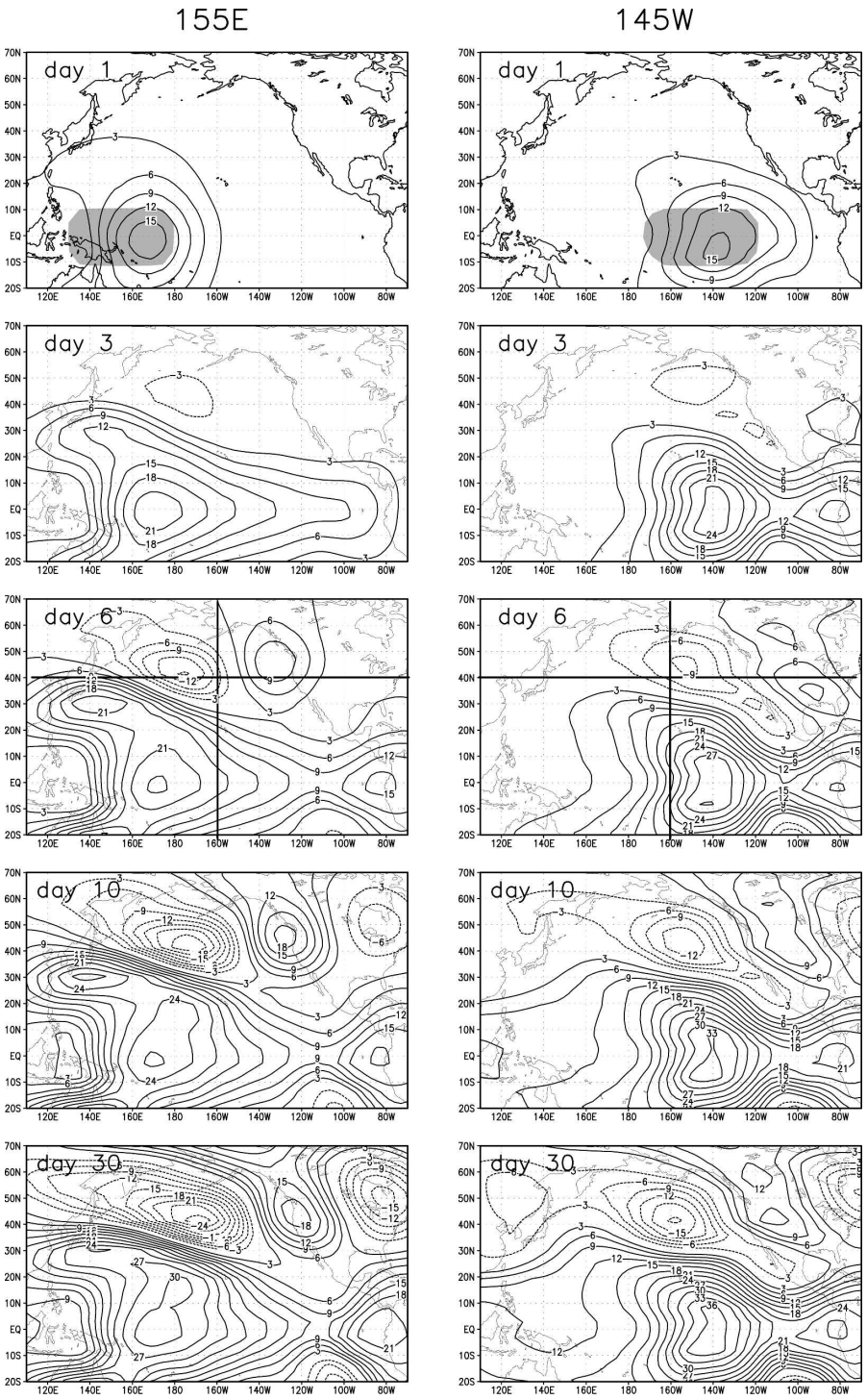

FIG. 11. Evolution of time-dependent LBM 200-hPa height response (unit: m) to an idealized tropical Pacific heating centered at (left) 155°E and (right) 145°W along the equator. The response on days 1, 3, 6, 10, and 30 is displayed, respectively. The shadings in the top panels indicate the location of the heating. The heating has a vertical maximum around 400 hPa and a maximum in-depth average rate of 4 K day^{-1}. In day-6 plots, the longitude 160°W and the latitude 40°N are drawn in solid line for comparison of North Pacific response location between the two heating cases. The contour 0 is omitted.

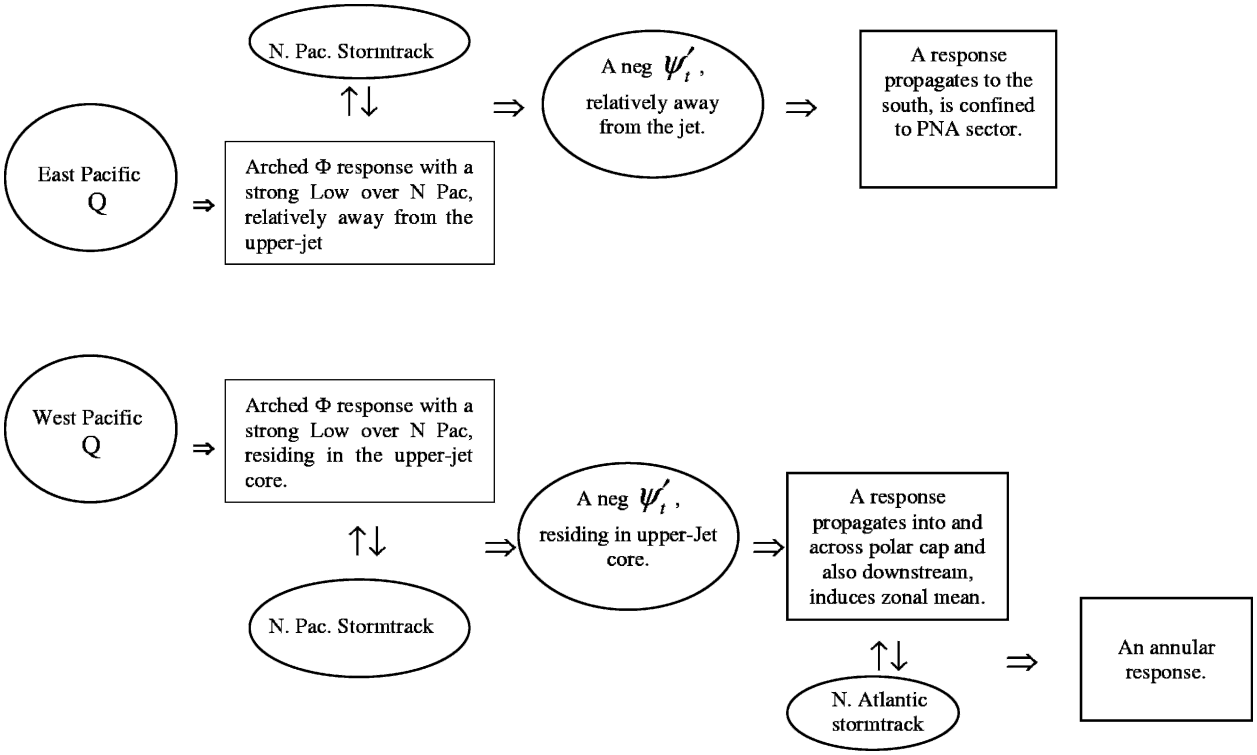

FIG. 12. Schematic diagram of mechanisms for two different responses to the tropical west and east Pacific forcing. The meanings of symbols are below: single-direction means "induce," double-direction arrow means "two-way interaction," "Q" heating, "Φ" geopotential height, "ψ_t'" transient eddy forcing expressed by streamfunction tendency, "pos" positive, "neg" negative, and "N. Pac." North Pacific.

are two orders of magnitude smaller than the basic flow.

Finally, Branstator emphasized the role of barotropic processes in inducing the annular pattern. Here we have focused on modulation of baroclinic eddies with time scales of less than 9 days. The life cycle of these eddies includes a decaying barotropic stage. A systematic relocation of this stage may contribute to the Pacific transient forcing. Further studies on changes in the life cycle of baroclinic eddies under 155°E and 145°W SSTA forcing are warranted.

Acknowledgments. We are grateful to Dr. Walter A. Robinson for helpful discussions on tropical heating influence on the extratropics, and to Dr. Jeffrey Whitaker for providing the linear baroclinic model. This research is supported in part by funding from the NOAA's CLIVAR Atlantic program.

REFERENCES

Ambaum, M. H. P., B. J. Hoskins, and D. B. Stephenson, 2001: Arctic Oscillation or North Atlantic Oscillation? *J. Climate,* **14,** 3495–3507.

Barsugli, J. J., and P. Sardeshmukh, 2002: Global atmospheric sensitivity to tropical SST anomalies throughout the Indo-Pacific basin. *J. Climate,* **15,** 3427–3442.

Branstator, G., 1992: The maintenance of low-frequency atmospheric anomalies. *J. Atmos. Sci.,* **49,** 1924–1945.

——, 2002: Circumglobal teleconnections, the jetstream waveguide, and the North Atlantic Oscillation. *J. Climate,* **15,** 1893–1910.

Cassou, C., and L. Terray, 2001: Oceanic forcing of the wintertime low-frequency atmospheric variability in the North Atlantic European sector: A study with the ARPEGE model. *J. Climate,* **14,** 4266–4291.

Deser, C., 2000: On the teleconnection activity of the "Arctic Oscillation." *Geophys. Res. Lett.,* **27,** 779–782.

Hall, N. M. J., J. Derome, and H. Lin, 2001: The extratropical signal generated by a midlatitude SST anomaly. Part I: Sensitivity at equilibrium. *J. Climate,* **14,** 2035–2053.

Hoerling, M. P., and A. Kumar, 2002: Atmospheric response patterns associated with tropical forcing. *J. Climate,* **15,** 2184–2203.

——, J. W. Hurrell, T. Xu, G. T. Bates, and A. S. Phillips, 2004: Twentieth century North Atlantic climate change. Part II: Understanding the effect of Indian Ocean warming. *Climate Dyn.,* **23,** 391–405.

Honda, M., H. Nakamura, J. Ukata, I. Kousaka, and K. Takeuchi, 2001: Interannual seesaw between the Aleutian and Icelandic Lows. Part I: Seasonal dependence and life cycle. *J. Climate,* **14,** 1029–1042.

Hoskins, B. J., and T. Ambrizzi, 1993: Rossby wave propagation

on a realistic longitudinally varying flow. *J. Atmos. Sci.,* **50,** 1661–1671.

Kalnay, E., and Coauthors, 1996: The NCEP/NCAR 40-Year Reanalysis Project. *Bull. Amer. Meteor. Soc.,* **77,** 437–471.

Lau, N.-C., and M. J. Nath, 1991: Variability of the baroclinic and barotropic transient eddy forcing associated with monthly changes in the midlatitude storm tracks. *J. Atmos. Sci.,* **48,** 2589–2613.

Li, S., 2004: Impact of Northwest Atlantic SST anomalies on the circulation over the Ural Mountains during early winter. *J. Meteor. Soc. Japan,* **82,** 971–988.

Mathieu, P.-P., R. T. Sutton, B. Tong, and M. Collins, 2004: Predictability of winter climate over the North Atlantic European region during ENSO events. *J. Climate,* **17,** 1953–1974.

Mo, K. C., and R. E. Livezey, 1986: Tropical–extratropical geopotential height teleconnections during the Northern Hemisphere winter. *Mon. Wea. Rev.,* **114,** 2488–2515.

Palmer, T., and D. Anderson, 1994: The prospects for seasonal forecasting—A review paper. *Quart. J. Roy. Meteor. Soc.,* **120,** 755–793.

Peng, S., and J. S. Whitaker, 1999: Mechanism determining the atmospheric response to midlatitude SST anomalies. *J. Climate,* **12,** 1393–1408.

——, and W. A. Robinson, 2001: Relationships between atmospheric internal variability and the responses to an extratropical SST anomaly. *J. Climate,* **14,** 2943–2959.

——, ——, and S. Li, 2002: North Atlantic SST forcing of the NAO and relationships with intrinsic hemispheric variability. *Geophys. Res. Lett.,* **29,** 1276, doi:10.1029/2001GL014043.

——, ——, and ——, 2003: Mechanisms for the linear and nonlinear NAO response to the North Atlantic SST tripole. *J. Climate,* **16,** 1987–2004.

——, ——, ——, and M. P. Hoerling, 2005: Tropical Atlantic SST forcing of coupled North Atlantic seasonal responses. *J. Climate,* **18,** 480–496.

Pozo-Vasquez, D., M. Esteban-Parra, F. Rodrigo, and Y. Castro-Diez, 2001: The association between ENSO and winter atmospheric circulation and temperature in the North Atlantic region. *J. Climate,* **14,** 3408–3420.

——, S. R. Gamiz-Fortis, J. Tovar-Pescador, M. Esteban-Parra, and Y. Castro-Diez, 2005: North Atlantic winter SLP anomalies based on the autumn ENSO state. *J. Climate,* **18,** 97–103.

Rasmusson, E. M., and T. H. Carpenter, 1982: Variations in tropical sea surface temperature and surface wind fields associated with the Southern Oscillation/El Niño. *Mon. Wea. Rev.,* **110,** 353–384.

Rayner, N. A., E. B. Horton, D. E. Parker, C. K. Folland, and R. B. Hackett, 1996: Version 2.2 of the global sea surface temperature data set, 1903–1994. Climate Research Tech. Note 74, Hadley Centre for Climate Prediction and Research, Met Office, 35 pp.

Rodwell, M. J., D. P. Rowell, and C. K. Folland, 1999: Oceanic forcing of the wintertime North Atlantic Oscillation and European climate. *Nature,* **398,** 320–323.

Rogers, J. C., 1997: North Atlantic storm track variability and its association to the North Atlantic Oscillation and climate variability of northern Europe. *J. Climate,* **10,** 1635–1647.

Sardeshmukh, P. D., and B. J. Hoskins, 1988: The generation of global rotational flow by steady, idealized tropical divergence. *J. Atmos. Sci.,* **45,** 1228–1251.

Sutton, R. T., and D. L. R. Hodson, 2003: Influence of the ocean on North Atlantic climate variability 1971–1999. *J. Climate,* **16,** 3296–3313.

——, W. A. Norton, and S. P. Jewson, 2000: The North Atlantic Oscillation—What role for the ocean? *Atmos. Sci. Lett.,* **1,** doi:10.1006/asle.2000.0021.

Thompson, D. W. J., and J. M. Wallace, 1998: The Arctic Oscillation signature in the wintertime geopotential height and temperature fields. *Geophys. Res. Lett.,* **25,** 1297–1300.

——, and ——, 2000: Annual modes in the extratropical circulation. Part I: Month-to-month variability. *J. Climate,* **13,** 1000–1016.

Ting, M., and P. D. Sardeshmukh, 1993: Factors determining the extratropical responses to equatorial diabatic heating anomalies. *J. Atmos. Sci.,* **50,** 907–918.

——, and L. Yu, 1998: Steady response to tropical heating in wavy linear and nonlinear baroclinic models. *J. Atmos. Sci.,* **55,** 3565–3582.

Trenberth, K. E., G. W. Branstator, D. Karoly, A. Kumar, N.-C. Lau, and C. Popelewski, 1998: Progress during TOGA in understanding and modeling global teleconnections associated with tropical sea surface temperatures. *J. Geophys. Res.,* **103,** 14 291–14 324.

Wallace, J. M., and D. W. J. Thompson, 2002: The Pacific center of action of the Northern Hemisphere annular mode: Real or artifact? *J. Climate,* **15,** 1987–1991.

Xie, P., and P. A. Arkin, 1997: Global precipitation: A 17-year monthly analysis based on gauge observations, satellite estimates, and numerical model outputs. *Bull. Amer. Meteor. Soc.,* **78,** 2539–2558.